Perturbative Quantum Monte Carlo Method for Nuclear Physics

Bing-Nan Lu,[1,*] Ning Li,[2] Serdar Elhatisari,[3] Yuan-Zhuo Ma,[4] Dean Lee,[5,†] and Ulf-G. Meißner[6,7,8,‡]

[1]*Graduate School of China Academy of Engineering Physics, Beijing 100193, China*
[2]*School of Physics, Sun Yat-Sen University, Guangzhou 510275, China*
[3]*Faculty of Natural Sciences and Engineering, Gaziantep Islam Science and Technology University, Gaziantep 27010, Turkey*
[4]*Guangdong Provincial Key Laboratory of Nuclear Science, Institute of Quantum Matter, South China Normal University, Guangzhou 510006, China*
[5]*Facility for Rare Isotope Beams and Department of Physics and Astronomy, Michigan State University, Michigan 48824, USA*
[6]*Helmholtz-Institut für Strahlen- und Kernphysik and Bethe Center for Theoretical Physics, Universität Bonn, D-53115 Bonn, Germany*
[7]*Institute for Advanced Simulation, Institut für Kernphysik, and Jülich Center for Hadron Physics, Forschungszentrum Jülich, D-52425 Jülich, Germany*
[8]*Tbilisi State University, 0186 Tbilisi, Georgia*

(Received 13 December 2021; revised 7 April 2022; accepted 2 June 2022; published 14 June 2022)

While first order perturbation theory is routinely used in quantum Monte Carlo (QMC) calculations, higher-order terms present significant numerical challenges. We present a new approach for computing perturbative corrections in projection QMC calculations. We demonstrate the method by computing nuclear ground state energies up to second order for a realistic chiral interaction. We calculate the binding energies of several light nuclei up to ^{16}O by expanding the Hamiltonian around the Wigner SU(4) limit and find good agreement with data. In contrast to the natural ordering of the perturbative series, we find remarkably large second-order energy corrections. This occurs because the perturbing interactions break the symmetries of the unperturbed Hamiltonian. Our method is free from the sign problem and can be applied to QMC calculations for many-body systems in nuclear physics, condensed matter physics, ultracold atoms, and quantum chemistry.

DOI: 10.1103/PhysRevLett.128.242501

Quantum Monte Carlo (QMC) simulation is a powerful method for addressing quantum many-body problems in nuclear physics [1–4], condensed matter [5–7], ultracold atoms [8–10], and quantum chemistry [11,12]. Perhaps the most important feature of QMC is that when the MC process has only positive weights, the computational effort scales only polynomially with system size. Unfortunately, this is not true in general. If the Monte Carlo process involves cancellations between positive and negative weights, the resulting "sign problem" leads to exponential scaling of the computational effort with system size. Although finding a generic solution for the sign problem is unlikely in the near term [13], for several important cases QMC algorithms can be applied without sign problems, such as lattice QCD at zero baryon density [14], the repulsive Fermi-Hubbard model at half filling [15], and low-energy nuclear systems in the Wigner SU(4) limit [16–19]. The realistic systems of physical interests, though, often deviate from these ideal models significantly and have a sign problem. In these cases, perturbation theory can be used to bridge the difference between the simplified and the realistic interaction. However, so far, perturbation theory in QMC is mostly limited to the first order. Improving the quality of the perturbative calculations requires going to higher orders.

In Rayleigh-Schrödinger perturbation theory, the second-order energy correction involves a summation over all quantum states that can be reached via the perturbing interaction. Such a calculation over all quantum states is not compatible with QMC, which targets only the lowest energy states. To solve this problem, we introduce a computational framework called perturbative QMC (ptQMC), which allows for the efficient calculation of higher-order perturbative corrections within the Euclidean time formalism. As a demonstration, we implement this method using nuclear lattice effective field theory (NLEFT) [3,4] and perform benchmark calculations of the binding energies of several nuclei.

NLEFT is a QMC method for nuclear *ab initio* calculations. We regularize the chiral nuclear force on a periodic cubic lattice and employ the auxiliary field MC method to simulate finite nuclei. The advantage of this approach is that many-body correlation effects such as clustering emerge automatically [20,21]. Because of the sign problem, early NLEFT calculations were limited to a few nuclei and specially designed interactions [22–27]. In most of the recent NLEFT calculations, the higher-order chiral interactions are included with first-order perturbation theory [28–32].

The nuclear Hamiltonian is $H = K + V_0 + V_C$, where $K = -\nabla^2/2m$ is the kinetic energy operator and $m = 938.92$ MeV is the nucleon mass. We use a lattice spacing of $a = 1.32$ fm. The interaction is split into a dominant term V_0 and a correction V_C. The ground state of H can be found by applying imaginary time projectors to a trial wave function $|\Psi_T\rangle$, $|\Psi\rangle = \lim_{L_t\to\infty} M^{L_t/2}|\Psi_T\rangle$, with $M = :e^{-a_t H}:$ the transfer matrix and a_t the temporal step. The colons denote normal ordering. Without loss of generality, we assume that both V_0 and V_C can be decomposed in terms of auxiliary fields. For example, using a simple contact interaction for V_0,

$$:e^{-\frac{1}{2}a_t C_0 \rho(\boldsymbol{n})^2}: \propto \int \mathcal{D}s :e^{-\frac{s(\boldsymbol{n})^2}{2} + \sqrt{-a_t C_0}\, s(\boldsymbol{n})\rho(\boldsymbol{n})}:, \quad (1)$$

with $\rho(\boldsymbol{n})$ as the nucleon density and $s(\boldsymbol{n})$ as a real auxiliary field. We further require that V_0 does not induce a sign problem. This is possible when V_0 is attractive with $C_0 < 0$, and each spin-up nucleon in $|\Psi_T\rangle$ is paired with a spin-down nucleon [33]. This is the case for the ground states of even-even nuclei. However, we can use a more general V_C that may have a sign problem. By decomposing V_C in the same manner, we have similar expressions for the density ρ_c and the corresponding auxiliary field c. For nonperturbative QMC calculations, we need to sample both s and c fields.

Under the assumption that V_C is small compared to V_0, we can expand $|\Psi\rangle$ in powers of V_C,

$$|\Psi\rangle = \lim_{L_t\to\infty} M^{L_t/2}|\Psi_T\rangle = |\Psi_0\rangle + |\delta\Psi_1\rangle + \mathcal{O}(V_C^2), \quad (2)$$

$$|\Psi_0\rangle = \lim_{L_t\to\infty} M_0^{L_t/2}|\Psi_T\rangle, \quad (3)$$

$$|\delta\Psi_1\rangle = \lim_{L_t\to\infty} \sum_{k=1}^{L_t/2} M_0^{L_t/2-k}(M - M_0)M_0^{k-1}|\Psi_T\rangle, \quad (4)$$

where $M_0 =: e^{-a_t(K+V_0)}:$ is the zeroth-order transfer matrix and we have omitted the $\mathcal{O}(a_t^2)$ terms. In Eq. (2) and what follows, we use the subscripts to denote the perturbative orders and the symbols with δ to represent the corrections. The normalized wave function is

$$|\Psi'\rangle = \frac{|\Psi\rangle}{\sqrt{\langle\Psi|\Psi\rangle}} = \frac{|\Psi_0\rangle}{\sqrt{\langle\Psi_0|\Psi_0\rangle}} + \frac{1}{\sqrt{\langle\Psi_0|\Psi_0\rangle}} \times \left[|\delta\Psi_1\rangle - \frac{\mathrm{Re}\langle\Psi_0|\delta\Psi_1\rangle}{\langle\Psi_0|\Psi_0\rangle}|\Psi_0\rangle\right] + \mathcal{O}(V_C^2), \quad (5)$$

where Re denotes the real part. Equation (5) can be used to calculate the expectation value of any operator up to $\mathcal{O}(V_C)$. A special case is the energy, for which δE_1 only depends on $|\Psi_0\rangle$. With $|\delta\Psi_1\rangle$ at hand, we can continue further to find δE_2. The partial energy contributions at each order are

$$E_0 = \langle\Psi_0|(K + V_0)|\Psi_0\rangle/\langle\Psi_0|\Psi_0\rangle, \quad (6)$$

$$\delta E_1 = \langle\Psi_0|V_C|\Psi_0\rangle/\langle\Psi_0|\Psi_0\rangle, \quad (7)$$

$$\delta E_2 = \mathrm{Re}(\langle\Psi_0|V_C|\delta\Psi_1\rangle - \delta E_1\langle\Psi_0|\delta\Psi_1\rangle)/\langle\Psi_0|\Psi_0\rangle, \quad (8)$$

where all matrix elements and overlaps can be expressed with the amplitudes

$$\mathcal{M}(O) = \langle\Psi_T|M_0^{L_t/2} O M_0^{L_t/2}|\Psi_T\rangle, \quad (9)$$

$$\mathcal{M}_k(O) = \langle\Psi_T|M_0^{L_t/2} O M_0^{L_t/2-k} M M_0^{k-1}|\Psi_T\rangle, \quad (10)$$

where $k = 1, 2, \ldots, L_t/2$. Here O is the operator inserted in the middle time step like 1, $K + V_0$ or V_C. In $\mathcal{M}_k(O)$ the kth copy of M_0 is replaced by the full transfer matrix M. The transfer matrices M_0 and M in these amplitudes are computed using the auxiliary field formalism.

The energies E_0 and δE_1 are just the expectation values $\langle O\rangle = \mathcal{M}(O)/\mathcal{M}(1)$ with $O = K + V_0$ or V_C. These can be calculated by sampling the auxiliary fields s in M_0 with standard algorithms [3,4]. For δE_2 we need to evaluate an integral over the auxiliary field c from the inserted M in $\mathcal{M}_k(O)$. For every sample $\{s_1, s_2, \ldots, s_{L_t}\}$ we have

$$\mathcal{M}_k(O) = \int \mathcal{D}c P(c + \bar{c})\langle\cdots O\cdots M(s_k, c + \bar{c})\cdots\rangle_T, \quad (11)$$

where the ellipses denote the transfer matrices $M_0(s_t)$ with $t \neq k$, $\langle\rangle_T$ is the expectation value in the state $|\Psi_T\rangle$, and $P(c)$ is the standard normal distribution. In Eq. (11) we have made a variable change $c \to \bar{c} + c$ with c real integral variables. Here $\bar{c}(\boldsymbol{n})$ is a constant field

$$\bar{c}(\boldsymbol{n}) = \frac{\partial}{\partial c(\boldsymbol{n})} \ln\langle\cdots M(s_k, c)\cdots\rangle_T\Big|_{c=0} = \sqrt{-a_t C}\langle\cdots :M_0(s_k)\rho_c(\boldsymbol{n}):\cdots\rangle_T/\mathcal{M}(1), \quad (12)$$

where the ellipses again represent the M_0's, and C is the coupling constant for the V_C term. Generally, $\bar{c}$ is a complex field, e.g., for repulsive interactions such as Coulomb we have $C > 0$, the square root in Eq. (12) introduces an imaginary factor i. In this case, the integrand in Eq. (11) contains nonzero phases that may induce a severe sign problem. The variable change in Eq. (11) serves to alleviate this problem [34]. To see this, we take the logarithm of the integrand in Eq. (11), expand the result near $c = 0$, and apply Eq. (12). We find that the terms linear in c and $\bar{c}$ that cause the sign problem cancel exactly and the integrand can be factorized as

$$\mathcal{M}_k(O) = \mathcal{M}(s)\exp\left(\frac{\bar{c}^2}{2}\right)\int \mathcal{D}c\,\exp\left(-\frac{c^2}{2}+\epsilon\right), \quad (13)$$

where we omit the summations over lattice sites, and ϵ is a residual term containing quadratic and higher powers of c. Because in $\mathcal{M}_k(s,c)$ a common factor $\sqrt{a_t}$ is attached to every c variable, ϵ is a small number of the order $\mathcal{O}(a_t)$. For sufficiently small a_t, Eq. (13) means that the integrand in Eq. (11) is a product of a normal distribution and a slowly varying function $\exp(\epsilon)$. We can use stochastic methods to evaluate Eq. (11) by sampling the c field with a standard normal distribution. This evaluation is unbiased and its uncertainty is determined by the variation of $\exp(\epsilon)$. In practice, we found that the variable change in Eq. (11) can reduce the statistical error by one order or more, see the Supplemental Material [35] for a demonstration.

We benchmark the ptQMC using a realistic nuclear chiral force with two- and three-body interactions up to N^{2}LO [47,48]. The two-body contact terms and the one-pion-exchange potential (OPEP) read

$$\begin{aligned} V_{2N} = {} & [B_1 + B_2(\boldsymbol{\sigma}_1\cdot\boldsymbol{\sigma}_2) + C_1 q^2 + C_2 q^2(\boldsymbol{\tau}_1\cdot\boldsymbol{\tau}_2) \\ & + C_3 q^2(\boldsymbol{\sigma}_1\cdot\boldsymbol{\sigma}_2) + C_4 q^2(\boldsymbol{\sigma}_1\cdot\boldsymbol{\sigma}_2)(\boldsymbol{\tau}_1\cdot\boldsymbol{\tau}_2) \\ & + C_5\frac{i}{2}(\boldsymbol{q}\times\boldsymbol{k})\cdot(\boldsymbol{\sigma}_1+\boldsymbol{\sigma}_2) + C_6(\boldsymbol{\sigma}_1\cdot\boldsymbol{q})(\boldsymbol{\sigma}_2\cdot\boldsymbol{q}) \\ & + C_7(\boldsymbol{\sigma}_1\cdot\boldsymbol{q})(\boldsymbol{\sigma}_2\cdot\boldsymbol{q})(\boldsymbol{\tau}_1\cdot\boldsymbol{\tau}_2)]f_{2N}(p_1,p_2,p_1',p_2') \\ & - \frac{g_A^2 f_\pi(q^2)}{4F_\pi^2}\left[\frac{(\boldsymbol{\sigma}_1\cdot\boldsymbol{q})(\boldsymbol{\sigma}_2\cdot\boldsymbol{q})}{q^2+M_\pi^2} + C_\pi'\boldsymbol{\sigma}_1\cdot\boldsymbol{\sigma}_2\right](\boldsymbol{\tau}_1\cdot\boldsymbol{\tau}_2), \quad (14) \end{aligned}$$

where $\boldsymbol{\sigma}_{1,2}(\boldsymbol{\tau}_{1,2})$ are spin (isospin) matrices, B_i and C_i are low-energy constants (LECs). $\boldsymbol{p}$ and $\boldsymbol{p}'$ are the relative incoming and outgoing momenta, respectively, $\boldsymbol{q} = \boldsymbol{p} - \boldsymbol{p}'$, $\boldsymbol{k} = (\boldsymbol{p}+\boldsymbol{p}')/2$ are momentum transfers, $\boldsymbol{p}_i$ and $\boldsymbol{p}_i'$ are the momenta of the individual nucleons, and g_A, F_π, and M_π are the axial-vector coupling constant, pion decay constant, and pion mass, respectively. The additional regulators, $f_{2N} = \exp[-\sum_{i=1}^{2}(p_i^6 + p_i'^6)/\Lambda^6]$ with $\Lambda = 340$ MeV and $f_\pi = \exp[-(q^2+M_\pi^2)/\Lambda_\pi^2]$ with $\Lambda_\pi = 300$ MeV, are introduced to minimize lattice artifacts. For the OPEP we introduce a counterterm $\sim C_\pi'$ as in Ref. [48] to remove the short-range singularity, which, together with a low Λ_π, adapts the potential to perturbative calculations. Note that the OPEP contains a tensor interaction that couples different partial waves, and thus will contribute significantly to the energy at second order. For the three-nucleon (3N) force V_{3N} we adopt a simple 3N contact term with the LEC c_E. The LECs B_i, C_i, and c_E are fixed from NN scattering data and the triton binding energy. We also implement a static Coulomb force V_{cou}, see Supplemental Material [35] for further details of the interaction.

In order to compute ground states of $H = K + V_{2N} + V_{3N} + V_{cou}$ using ptQMC, we shall choose a zeroth-order Hamiltonian $H_0 = K + V_0$ and calculate the energy corrections with respect to $V_C = H - H_0$. We take V_0 to be the nonlocally smeared SU(4) interaction from Ref. [19], which captures the essential elements of the nuclear force. For benchmarking purposes, we only keep the two-body part of V_0, which induces no sign problem for even-even nuclei. The details of V_0 can be found in the Supplemental Material [35]. For further work starting with the Wigner SU(4) limit, see [49–51].

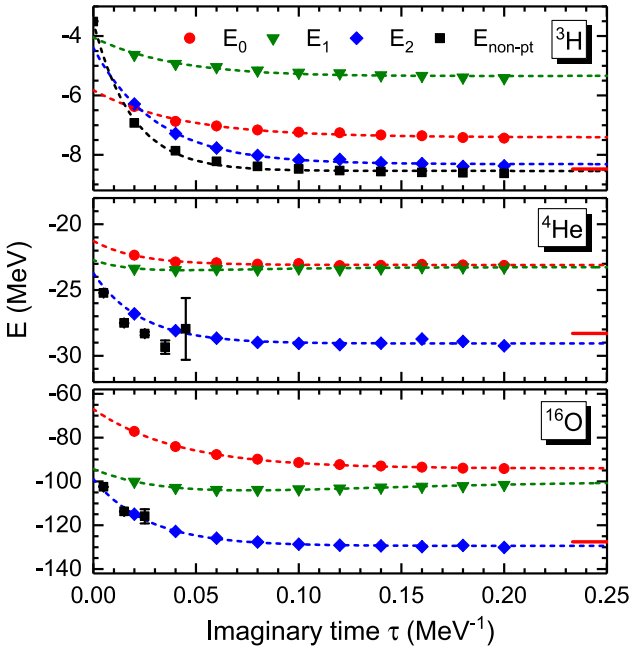

FIG. 1. ptQMC binding energies as functions of the projection time τ compared with nonperturbative results. The circles (red), down triangles (green), and diamonds (blue) denote the energies at the zeroth, first, and second orders, respectively. The squares (black) represent the exact results calculated with sparse matrix multiplications for ^{3}H and full nonperturbative QMC for ^{4}He and ^{16}O, respectively. Each group of results are fitted with a sum of exponential functions (dashed lines). The red bars mark the experimental binding energies.

In Fig. 1, we compare the results obtained using ptQMC with nonperturbative results. We use a periodic box of size $L = 10$ for ^{3}H and $L = 8$ for the other nuclei. The temporal step is $a_t = 1/1000$ MeV^{-1}. For ^{3}H, the system is small enough that we can use exact sparse matrix calculations. For larger nuclei we perform fully nonperturbative QMC calculations instead, which result in large error bars due to severe sign problems. For the ^{16}O nucleus, the sign problem sets in so quickly that we cannot find meaningful results to make a reliable extrapolation. However, the ptQMC calculations are free from sign problems. The corresponding statistical errors are smaller than the size of the symbols. We use a sum of decaying exponential functions to capture the residual effects of higher energy excitations and extrapolate the results to $\tau \to \infty$. See the Supplemental Material [35] for further settings of the QMC simulation.

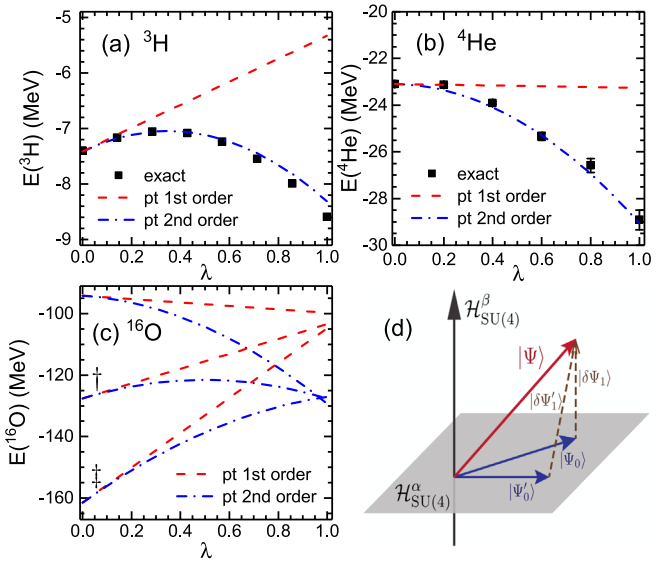

FIG. 2. (a),(b) The dashed and dash-dotted lines denote the binding energies of ^{3}H (a) and ^{4}He (b) as functions of the small parameter λ in first- and second-order ptQMC calculations, respectively. The black squares are the exact results. (c) The first- and second-order ptQMC calculations for ^{16}O, starting from three different zeroth-order interactions V_0, $1.1V_0$ (†), and $1.2V_0$ (‡). (d) Schematic plot for a perturbative calculation. The zeroth-order wave functions $|\Psi_0\rangle$ and $|\Psi'_0\rangle$ are confined in a subspace corresponding to an IR of SU(4).

For all three nuclei, the second-order energy corrections are large and essential in reproducing the data. While this might seem contrary to the normal hierarchy of the perturbative series, we will show below that it is actually a consequence of the symmetry breaking.

We can now examine the convergence pattern of the perturbative series. In Figs. 2(a)–2(c), we show the calculated energies as a function of λ, a real number between 0 and 1 that we insert as a control parameter multiplying the perturbation V_C. The ptQMC results are shown as lines. Because ptQMC corresponds to the Taylor series expansion at $\lambda = 0$, we find straight lines at first and parabolas at second order. For ^{3}H (^{4}He) we also display the exact energies of $H_0 + \lambda V_C$ obtained with sparse matrix diagonalization (full nonperturbative QMC). The difference between the second-order and exact results indicate the contributions from the third and higher orders, which are more than 1 order smaller in magnitude.

For ^{16}O we cannot obtain nonperturbative results for benchmarking due to the severe sign problem, and so instead we vary the zeroth-order Hamiltonian to triangulate the binding energy and estimate its uncertainty. In Fig. 2(c), the † and ‡ symbols mark the ptQMC energies calculated with $H_0 = K + 1.1V_0$ and $H_0 = K + 1.2V_0$, respectively. For each calculation, we use $V_C = H - H_0$ as the perturbing Hamiltonian and plot the energies as functions of the small parameter λ. While the variation of H_0 shifts the zeroth-order energy by about 50 MeV, for full Hamiltonian H ($\lambda = 1$) we find that the first- and second-order energies only vary by about 4 and 2.4 MeV, respectively. These variations can be identified as the truncation errors of the perturbative series at corresponding orders, see also the Supplemental Material [35].

TABLE I. Binding energies at different orders calculated with ptQMC compared to experiment (all in MeV). The errors are combinations of MC statistical errors and extrapolation errors [35]. See Fig. 2(c) for further notations.

	E_0	δE_1	E_1	δE_2	E_2	$E_{\rm exp}$
^{3}H	−7.41(3)	+2.08	−5.33(3)	−2.99	−8.32(3)	−8.48
^{4}He	−23.1(0)	−0.2	−23.3(0)	−5.8	−29.1(1)	−28.3
^{8}Be	−44.9(4)	−1.7	−46.6(4)	−11.1	−57.7(4)	−56.5
^{12}C	−68.3(4)	−1.8	−70.1(4)	−18.8	−88.9(3)	−92.2
^{16}O	−94.1(2)	−5.6	−99.7(2)	−29.7	−129.4(2)	−127.6
^{16}O†	−127.6(4)	+24.2	−103.4(4)	−24.3	−127.7(2)	−127.6
^{16}O‡	−161.5(1)	+56.8	−104.7(2)	−22.3	−127.0(2)	−127.6

In Table I we present the ptQMC energies for several nuclei compared to the empirical values. The improvement of E_2 compared with E_1 is clearly seen. Generally, the correlation energy δE_2 accounts for about 20% of the total binding energy for all nuclei with $A \geq 4$. We note that the first-order energy is the expectation value of the full Hamiltonian using the zeroth-order wave function $|\Psi_0\rangle$, and it is an upper bound on the ground state energy. The energy correction δE_2 is negative definite, reflecting the fact that the corrected wave function $|\Psi_1\rangle$ is much closer to the exact ground state than $|\Psi_0\rangle$.

In perturbative calculations, the convergence pattern can be invalidated by symmetry constraints. As the unperturbed Hamiltonian H_0 respects the SU(4) symmetry, the wave function $|\Psi_0\rangle$ must belong to one of its irreducible representations (IRs). The full Hamiltonian breaks the SU(4) symmetry, thus its ground state $|\Psi\rangle$ is a mixture of different SU(4) IRs. As is shown in Fig. 2(d), the components of $|\Psi\rangle$ that mix the SU(4) IRs can only be seen in $|\delta\Psi_1\rangle$ or δE_2. This explains the large δE_2 in ^{16}O that cannot be eliminated by varying H_0. We note that this effect is strongest for the OPEP in Eq. (14) as it breaks both the Wigner SU(4) and the spin SU(2) symmetries.

In summary, we have presented a novel algorithm (ptQMC) that allows for a precise calculation of the second-order perturbative correction in QMC without referring to the full spectrum of the excited states. While the QMC method with simplified interactions is successfully applied in various fields of physics [19,52–62], attempts to use more realistic interactions are hindered by the sign problem. The ptQMC method is free from sign problems and opens the way to treat complex interactions systematically. Our method converges quickly for relatively soft interactions. For interactions with strong short-distance

correlations such as tensor forces, which are important in electroweak processes [63], some preprocessing of the interaction using renormalization group transformations or some analogous method is required.

We are grateful for discussions with members of the Nuclear Lattice Effective Field Theory Collaboration. We gratefully acknowledge funding by NSAF (Grant No. U1930403), the Deutsche Forschungsgemeinschaft (DFG, German Research Foundation), and the NSFC through the funds provided to the Sino-German Collaborative Research Center TRR110 "Symmetries and the Emergence of Structure in QCD" (DFG Project ID 196253076—TRR 110, NSFC Grant No. 12070131001), the Chinese Academy of Sciences (CAS) President's International Fellowship Initiative (PIFI) (Grant No. 2018DM0034), Volkswagen Stiftung (Grant No. 93562), the European Research Council (ERC) under the European Union's Horizon 2020 research and innovation program (Grant Agreement No. 101018170), the U.S. Department of Energy (DE-SC0013365 and DE-SC0021152), the Nuclear Computational Low-Energy Initiative (NUCLEI) SciDAC-4 project (DE-SC0018083), the Scientific and Technological Research Council of Turkey (TUBITAK Project No. 120F341), the National Natural Science Foundation of China under Grant No. 12105106, and the China Postdoctoral Science Foundation under Grants No. BX20200136 and No. 2020M682747, as well as computational resources provided by the Beijing Super Cloud Computing Center (BSCC, [64]), TianHe 3F, the Gauss Centre for Supercomputing e.V. [65] for computing time on the GCS Supercomputer JUWELS at Jülich Supercomputing Centre (JSC) and the Oak Ridge Leadership Computing Facility through the INCITE award "Ab-initio nuclear structure and nuclear reactions". Further computational resources from the JSC on JURECA D. C. are gratefully acknowledged.

*bnlv@gscaep.ac.cn
†lee.dean.j@gmail.com
‡meissner@hiskp.uni-bonn.de

[1] K. Langanke, D. J. Dean, P. B. Radha, Y. Alhassid, and S. E. Koonin, Phys. Rev. C **52**, 718 (1995).
[2] J. Carlson, S. Gandolfi, F. Pederiva, Steven C. Pieper, R. Schiavilla, K. E. Schmidt, and R. B. Wiringa, Rev. Mod. Phys. **87**, 1067 (2015).
[3] D. Lee, Prog. Part. Nucl. Phys. **63**, 117 (2009).
[4] T. A. Lähde and U.-G. Meißner, Lect. Notes Phys. **957**, 1 (2019).
[5] D. M. Ceperley and B. J. Alder, Phys. Rev. Lett. **45**, 566 (1980).
[6] W. M. C. Foulkes, L. Mitas, R. J. Needs, and G. Rajagopal, Rev. Mod. Phys. **73**, 33 (2001).
[7] F. F. Assaad and I. F. Herbut, Phys. Rev. X **3**, 031010 (2013).
[8] A. Bulgac, J. E. Drut, and P. Magierski, Phys. Rev. A **78**, 023625 (2008).
[9] J. Carlson, S. Gandolfi, K. E. Schmidt, and S. Zhang, Phys. Rev. A **84**, 061602(R) (2011).
[10] R. He, N. Li, B. N. Lu, and D. Lee, Phys. Rev. A **101**, 063615 (2020).
[11] B. J. Hammond, W. A. Lester, and P. J. Reynolds, *Monte Carlo Methods in Ab Initio Quantum Chemistry* (World Scientific, Singapore, 1994).
[12] M. Nightingale and C. Umrigar, *Quantum Monte Carlo Methods in Physics and Chemistry* (Springer, New York, 1999); NNDC, Nudat 2 (2014), http://www.nndc.bnl.gov/nudat2/chartNuc.jsp.
[13] M. Troyer and U.-J. Wiese, Phys. Rev. Lett. **94**, 170201 (2005).
[14] S. Muroya, A. Nakamura, C. Nonaka, and T. Takaishi, Prog. Theor. Phys. **110**, 615 (2003).
[15] C. N. Varney, C.-R. Lee, Z. J. Bai, S. Chiesa, M. Jarrell, and R. T. Scalettar, Phys. Rev. B **80**, 075116 (2009).
[16] E. Wigner, Phys. Rev. **51**, 106 (1937).
[17] S. Elhatisari, N. Li, A. Rokash, J. M. Alarcón, D. Du, N. Klein, B.-N. Lu, Ulf-G. Meißner, E. Epelbaum, H. Krebs, T. A. Lähde, D. Lee, and G. Rupak, Phys. Rev. Lett. **117**, 132501 (2016).
[18] D. Lee, S. Bogner, B. A. Brown, S. Elhatisari, E. Epelbaum, H. Hergert, M. Hjorth-Jensen, H. Krebs, N. Li, B.-N. Lu, and Ulf-G. Meißner, Phys. Rev. Lett. **127**, 062501 (2021).
[19] B.-N. Lu, N. Li, S. Elhatisari, D. Lee, E. Epelbaum, and U.-G. Meißner, Phys. Lett. B **797**, 134863 (2019).
[20] S. Elhatisari, E. Epelbaum, H. Krebs, T. A. Lähde, D. Lee, N. Li, B.-N. Lu, Ulf-G. Meißner, and G. Rupak, Phys. Rev. Lett. **119**, 222505 (2017).
[21] N. Summerfield, B.-N. Lu, C. Plumberg, D. Lee, J. Noronha-Hostler, and A. Timmins, Phys. Rev. C **104**, L041901 (2021).
[22] B. Borasoy, E. Epelbaum, H. Krebs, D. Lee, and U.-G. Meißner, Eur. Phys. J. A **31**, 105 (2007).
[23] B. Borasoy, E. Epelbaum, H. Krebs, D. Lee, and U.-G. Meißner, Eur. Phys. J. A **35**, 343 (2008).
[24] E. Epelbaum, H. Krebs, D. Lee, and U.-G. Meißner, Eur. Phys. J. A **41**, 125 (2009).
[25] E. Epelbaum, H. Krebs, D. Lee, and Ulf-G. Meißner, Phys. Rev. Lett. **104**, 142501 (2010).
[26] E. Epelbaum, H. Krebs, D. Lee, and U.-G. Meißner, Eur. Phys. J. A **45**, 335 (2010).
[27] T. A. Lähde, E. Epelbaum, H. Krebs, D. Lee, U.-G. Meißner, and G. Rupak, Phys. Lett. B **732**, 110 (2014).
[28] E. Epelbaum, H. Krebs, D. Lee, and Ulf-G. Meißner, Phys. Rev. Lett. **106**, 192501 (2011).
[29] E. Epelbaum, H. Krebs, T. A. Lähde, D. Lee, and Ulf-G. Meißner, Phys. Rev. Lett. **109**, 252501 (2012).
[30] E. Epelbaum, H. Krebs, T. A. Lähde, D. Lee, and Ulf-G. Meißner, Phys. Rev. Lett. **110**, 112502 (2013).
[31] E. Epelbaum, H. Krebs, T. A. Lähde, D. Lee, Ulf-G. Meißner, and G. Rupak, Phys. Rev. Lett. **112**, 102501 (2014).
[32] S. Elhatisari, D. Lee, G. Rupak, E. Epelbaum, H. Krebs, T. A. Lähde, T. Luu, and U.-G. Meißner, Nature (London) **528**, 111 (2015).

[33] Z. X. Li, Y. F. Jiang, and H. Yao, Phys. Rev. Lett. **117**, 267002 (2016).
[34] S. Zhang and H. Krakauer, Phys. Rev. Lett. **90**, 136401 (2003).
[35] See Supplemental Material at http://link.aps.org/supplemental/10.1103/PhysRevLett.128.242501, which contains details on the interaction, trial wave functions, imaginary time extrapolation, the perturbative expansion beyond second order, and methods to better estimate the theoretical uncertainties, which includes Refs. [19,36–46].
[36] V. G. J. Stoks, R. A. M. Klomp, M. C. M. Rentmeester, and J. J. de Swart, Phys. Rev. C **48**, 792 (1993).
[37] N. Li, S. Elhatisari, E. Epelbaum, D. Lee, B.-N. Lu, and Ulf-G. Meißner, Phys. Rev. C **98**, 044002 (2018).
[38] B.-N. Lu, T. A. Lähde, D. Lee, and U.-G. Meißner, Phys. Lett. B **760**, 309 (2016).
[39] A. Gezerlis, I. Tews, E. Epelbaum, S. Gandolfi, K. Hebeler, A. Nogga, and A. Schwenk, Phys. Rev. Lett. **111**, 032501 (2013).
[40] P. Reinert, H. Krebs, and E. Epelbaum, Eur. Phys. J. A **54**, 86 (2018).
[41] E. Epelbaum, W. Glöckle, and U.-G. Meißner, Nucl. Phys. **A747**, 362 (2005).
[42] E. Epelbaum, H. Krebs, and U.-G. Meißner, Eur. Phys. J. A **51**, 53 (2015).
[43] S. Binder *et al.* (LENPIC Collaboration), Phys. Rev. C **93**, 044002 (2016).
[44] R. J. Furnstahl, N. Klco, D. R. Phillips, and S. Wesolowski, Phys. Rev. C **92**, 024005 (2015).
[45] J. A. Melendez, S. Wesolowski, and R. J. Furnstahl, Phys. Rev. C **96**, 024003 (2017).
[46] E. Epelbaum, J. Golak, K. Hebeler, H. Kamada, H. Krebs, U.-G. Meißner, A. Nogga, P. Reinert, R. Skibiński, K. Topolnicki, Y. Volkotrub, and H. Witała, Eur. Phys. J. A **56**, 92 (2020).
[47] E. Epelbaum, H.-W. Hammer, and Ulf-G. Meißner, Rev. Mod. Phys. **81**, 1773 (2009).
[48] P. Reinert, H. Krebs, and E. Epelbaum, Eur. Phys. J. A **54**, 86 (2018).
[49] S. König, H. W. Grießhammer, H.-W. Hammer, and U. van Kolck, Phys. Rev. Lett. **118**, 202501 (2017).
[50] S. König, Eur. Phys. J. A **56**, 113 (2020).
[51] J. Vanasse and D. R. Phillips, Few-Body Syst. **58**, 26 (2017).
[52] R. B. Wiringa and S. C. Pieper, Phys. Rev. Lett. **89**, 182501 (2002).
[53] A. W. Sandvik, Phys. Rev. Lett. **98**, 227202 (2007).
[54] L. Wang, Y. H. Liu, M. Iazzi, M. Troyer, and G. Harcos, Phys. Rev. Lett. **115**, 250601 (2015).
[55] Z. C. Wei, C. J. Wu, Y. Li, S. W. Zhang, and T. Xiang, Phys. Rev. Lett. **116**, 250601 (2016).
[56] Z. X. Li, Y. F. Jiang, and H. Yao, Phys. Rev. Lett. **117**, 267002 (2016).
[57] C. J. Wu, J. P. Hu, and S. C. Zhang, Phys. Rev. Lett. **91**, 186402 (2003).
[58] C. J. Wu and S. C. Zhang, Phys. Rev. B **71**, 155115 (2005).
[59] A. Bulgac, J. E. Drut, and P. Magierski, Phys. Rev. Lett. **96**, 090404 (2006).
[60] A. Richie-Halford, J. E. Drut, and A. Bulgac, Phys. Rev. Lett. **125**, 060403 (2020).
[61] C. J. Umrigar, J. Toulouse, C. Filippi, S. Sorella, and R. G. Hennig, Phys. Rev. Lett. **98**, 110201 (2007).
[62] D. Hangleiter, I. Roth, D. Nagaj, and J. Eisert, Sci. Adv. **6**, eabb8341 (2020).
[63] J. Menéndez, D. Gazit, and A. Schwenk, Phys. Rev. Lett. **107**, 062501 (2011).
[64] http://www.blsc.cn/.
[65] www.gauss-centre.eu.